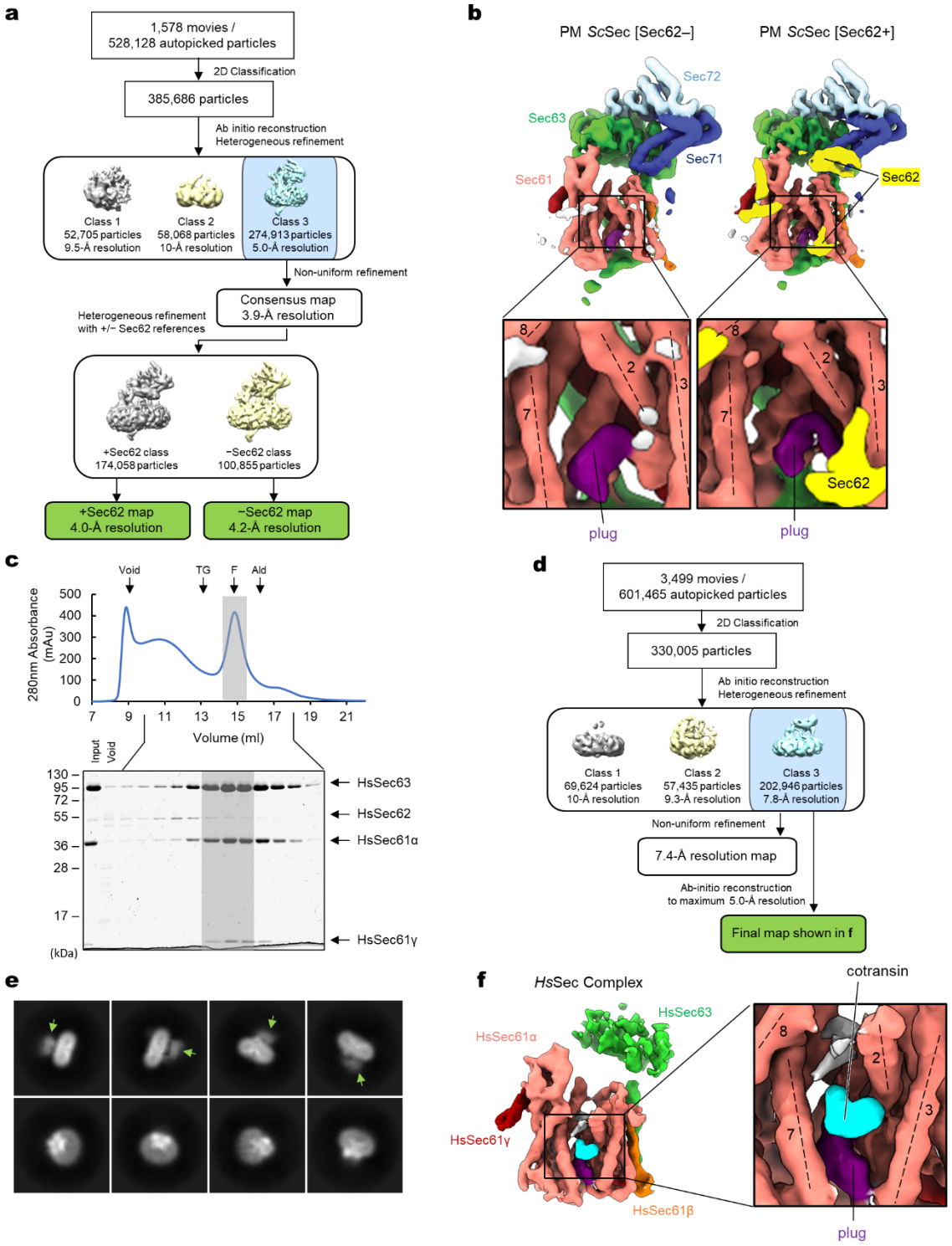

Supplementary Figure S1. Cryo-EM analysis of the yeast and human Sec complexes.
a, A schematic of the single-particle cryo-EM analysis of the yeast Sec (*Sc*Sec) complex incubated with cotransin. Note that the particles were sorted into two 3D classes, with and without Sec62, due to partial occupancy of Sec62. **b**, 3D reconstructions of the *Sc*Sec complex with and without *Sc*Sec62 (shown in yellow). No cotransin-like density was observed in either class. For this experiment, we used a pore ring mutant (PM; M90L/T185I/M294I/M450L) that stabilize the plug towards a closed conformation (ref. 17). **c**, Purification of the human Sec (*Hs*Sec) complex. Shown is a Superose 6 size-exclusion chromatography elution profile with fractions analyzed on a Coomassie-stained SDS gel. Note that under the used purification condition, *Hs*Sec62 does not co-purify at a stoichiometric ratio or stably comigrate with the Sec61–Sec63 complex. The fractions indicated by gray shade were used for cryo-EM. MW standards: Tg, thyroglobulin; F, ferritin; Ald, aldolase. **d**, A schematic of the single-particle analysis of *Hs*Sec complex incubated with cotransin. Due to a poor refinement result from nonuniform refinement in cryoSPARC, the final reconstruction was obtained by the ab-initio refinement function of cryoSPARC (see **f**). **e**, Representative 2D classes of the *Hs*Sec complex. Diffuse cytosolic features of Sec63 (green arrowheads) suggest its flexibility or disorderedness. **f**, The 3D reconstruction of the *Hs*Sec complex. A putative cotransin feature (cyan) is visible at the lateral gate.

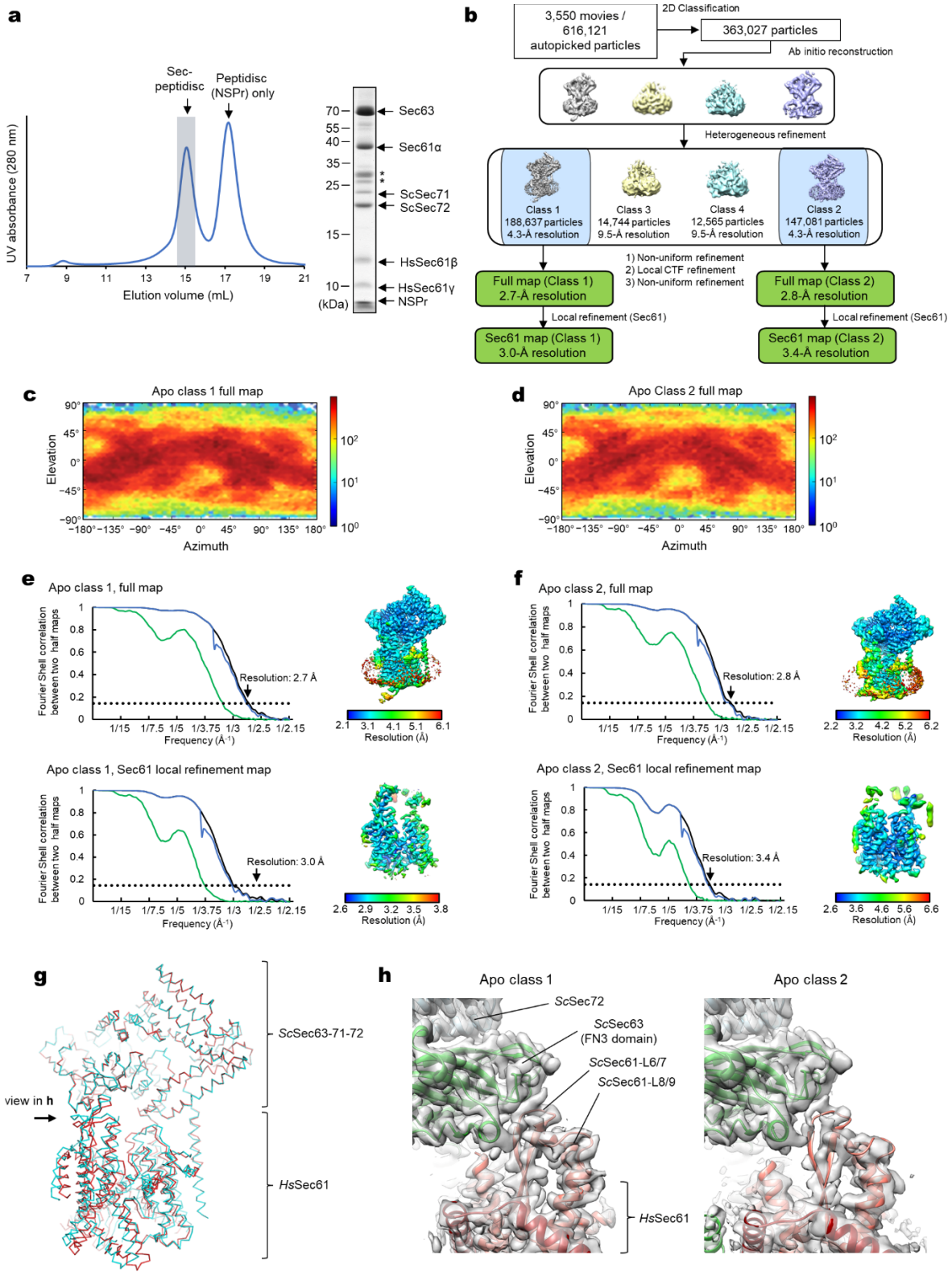

Supplementary Figure S2. Cryo-EM analysis of the chimeric Sec complex in an apo form.
a, Purification of the chimeric Sec complex reconstituted in a peptidisc. Left, Superose 6 elution profile; right, Coomassie-stained SDS gel of the peak fraction. The fraction marked by gray shade was used for cryo-EM. Asterisks, putative species of glycosylated *Sc*Sec71. **b**, A schematic of the cryo-EM analysis of the chimeric Sec complex in an apo state. **c** and **d**, Distributions of particle view orientations in the final reconstructions of Classes 1 (c) and 2 (d). **e** and **f**, Fourier shell correlation (FSC) curves and local resolution maps of the final reconstructions. **g**, Superimposition of the Class 1 and 2 atomic models (based on the cytosolic domains) shows a slight difference in relative positions between Sec63-Sec71-Sec72 and the Sec61 complex. **h**, Side views showing the contact between the engineered cytosolic loops of Sec61α and the FN3 domain of *Sc*Sec63. Note that in Apo Class 2, the contact is more poorly packed than Class 1.

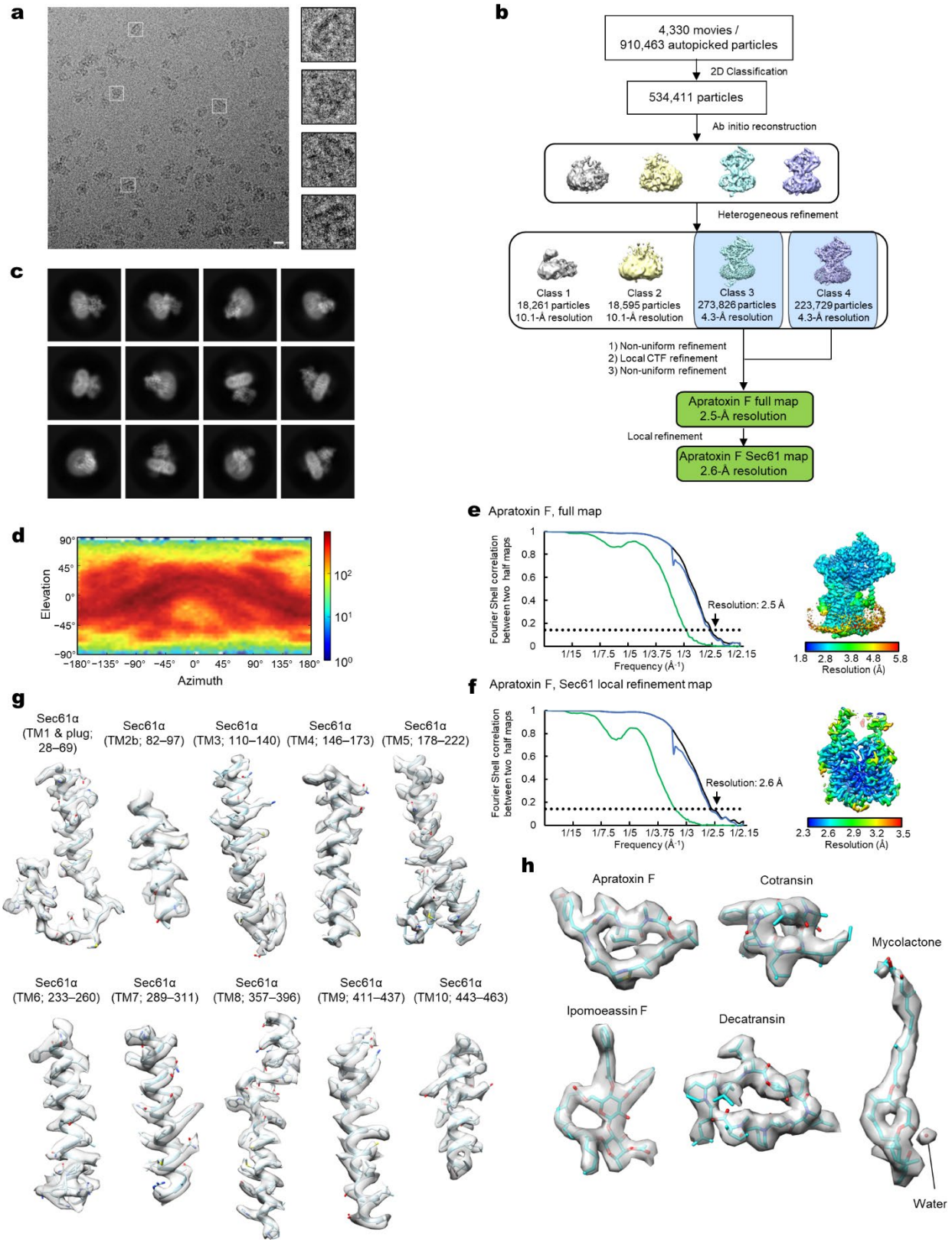

Supplementary Figure S3. Cryo-EM analysis of the chimeric Sec complex in an inhibitor (apratoxin F)-bound form.
a, Images of a representative micrograph and particles of the apratoxin F-bound chimeric Sec complex. Scale bar, 10 nm. **b**, A schematic of the cryo-EM analysis of the apratoxin F-bound chimeric Sec complex. **c**, Representative 2D classes of the apratoxin F-bound Sec complex. **d**, Distribution of particle view orientations in the final reconstruction. **e**, The FSC curve and local resolution map of the final reconstruction (full Sec complex map). **f**, As in e, but for the map from focused (local) refinement. **g**, Segmented density maps of the apratoxin F-bound Sec61α subunit. **h**, Segmented density features of bound natural inhibitors.

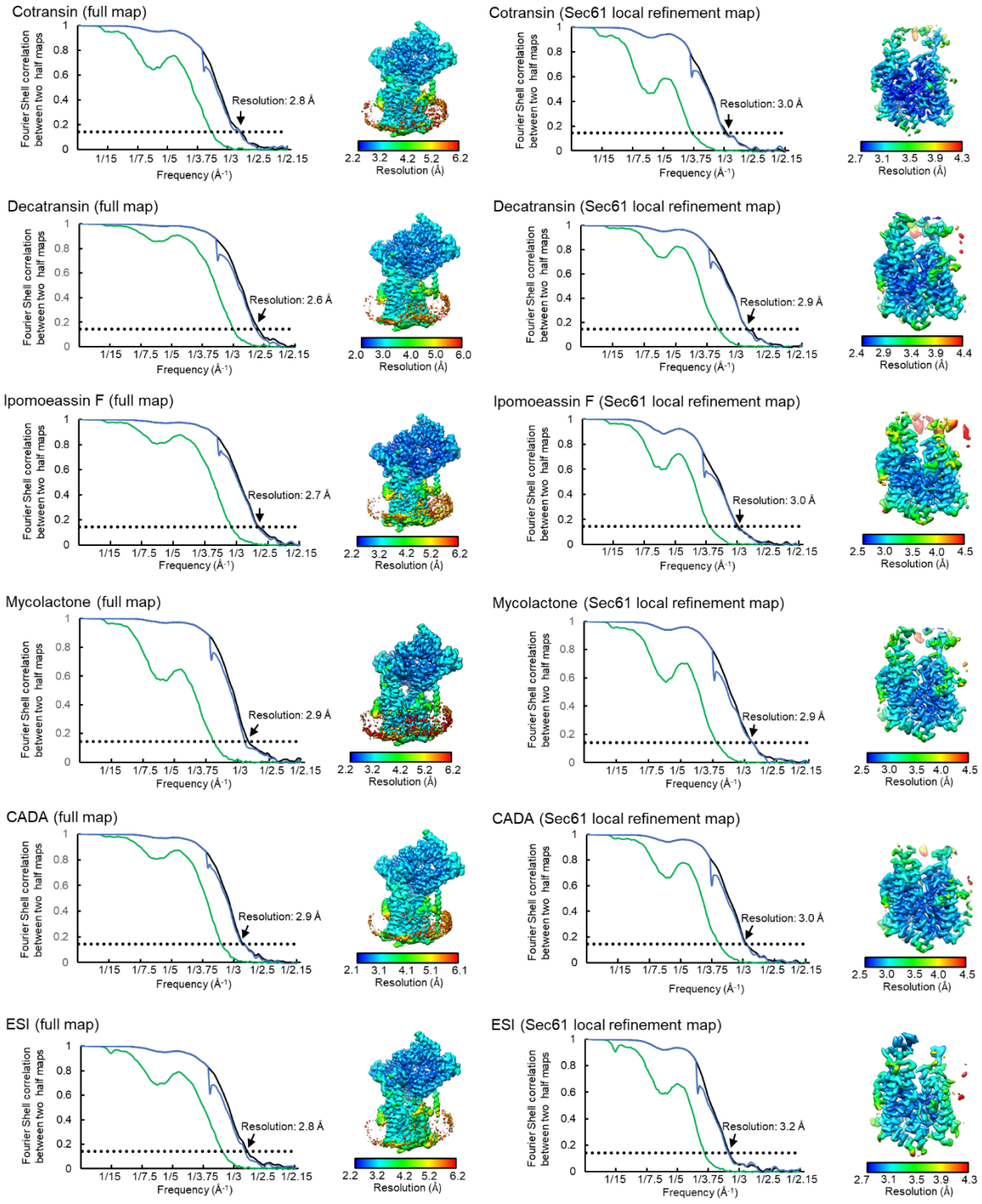

Supplementary Figure S4. FSC curve and local resolution maps of inhibitor-bound Sec complexes.
As in Supplementary Figure S3 e and f, but for all other inhibitor-bound structures.

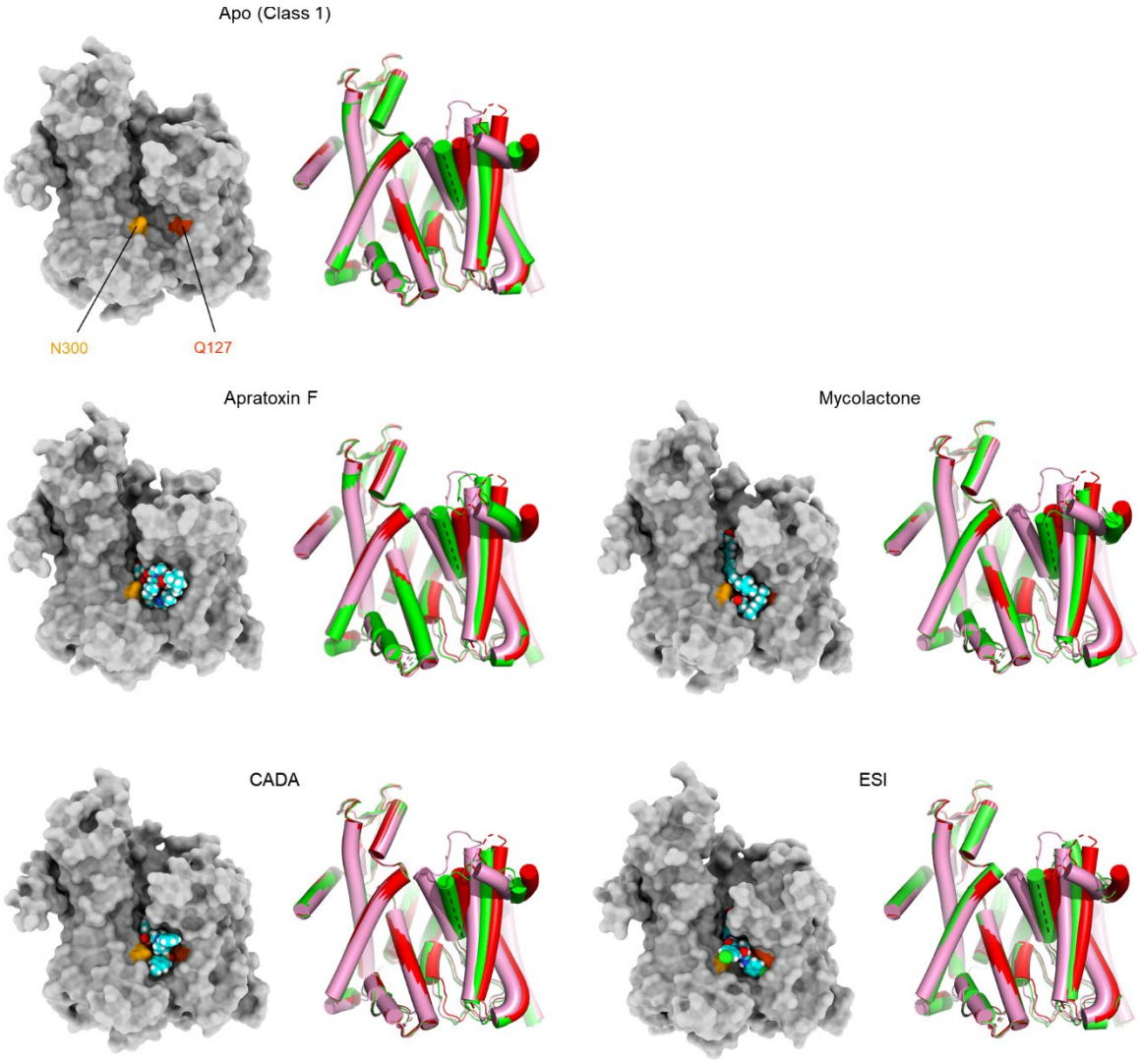

Supplementary Figure S5. Variation in the extent of lateral gate opening in inhibitor-bound structures.
As in Fig. 2 a and b, but showing other inhibitor-bound structures. In all panels showing a lateral gate comparison, cylindrical representations in red and pink are the cotransin- and ipomoeassin F- bound structures, respectively, whereas the representation in green is the structure with the indicated inhibitor.

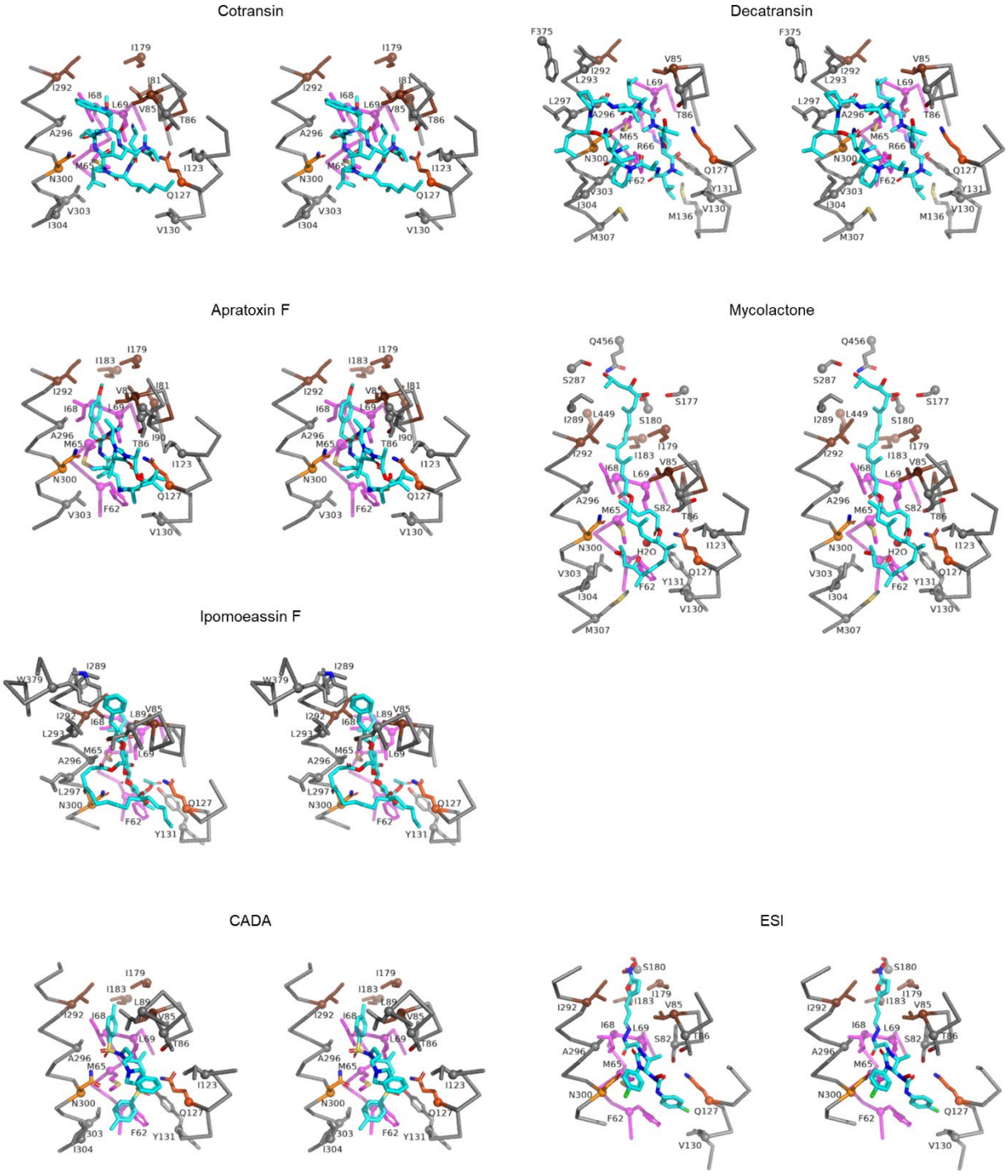

Supplementary Figure S6. 3-D maps for interactions between Sec61 and inhibitors.
Shown are stereo-views into the inhibitor-binding site. Inhibitors and adjacent protein side chains are shown in a stick representation together with Cα traces for TM2b, TM3, TM7, and the plug. The views are roughly similar between the different structures but adjusted for each structure for more clear representations. The following colors are used to differentiate parts: brown, pore ring residues; magenta, plug; lighter orange; N300, darker orange, Q127. All inhibitors are shown in cyan with certain atom-dependent coloring (nitrogen-blue, oxygen-red, sulfur-yellow, and chlorine-green).

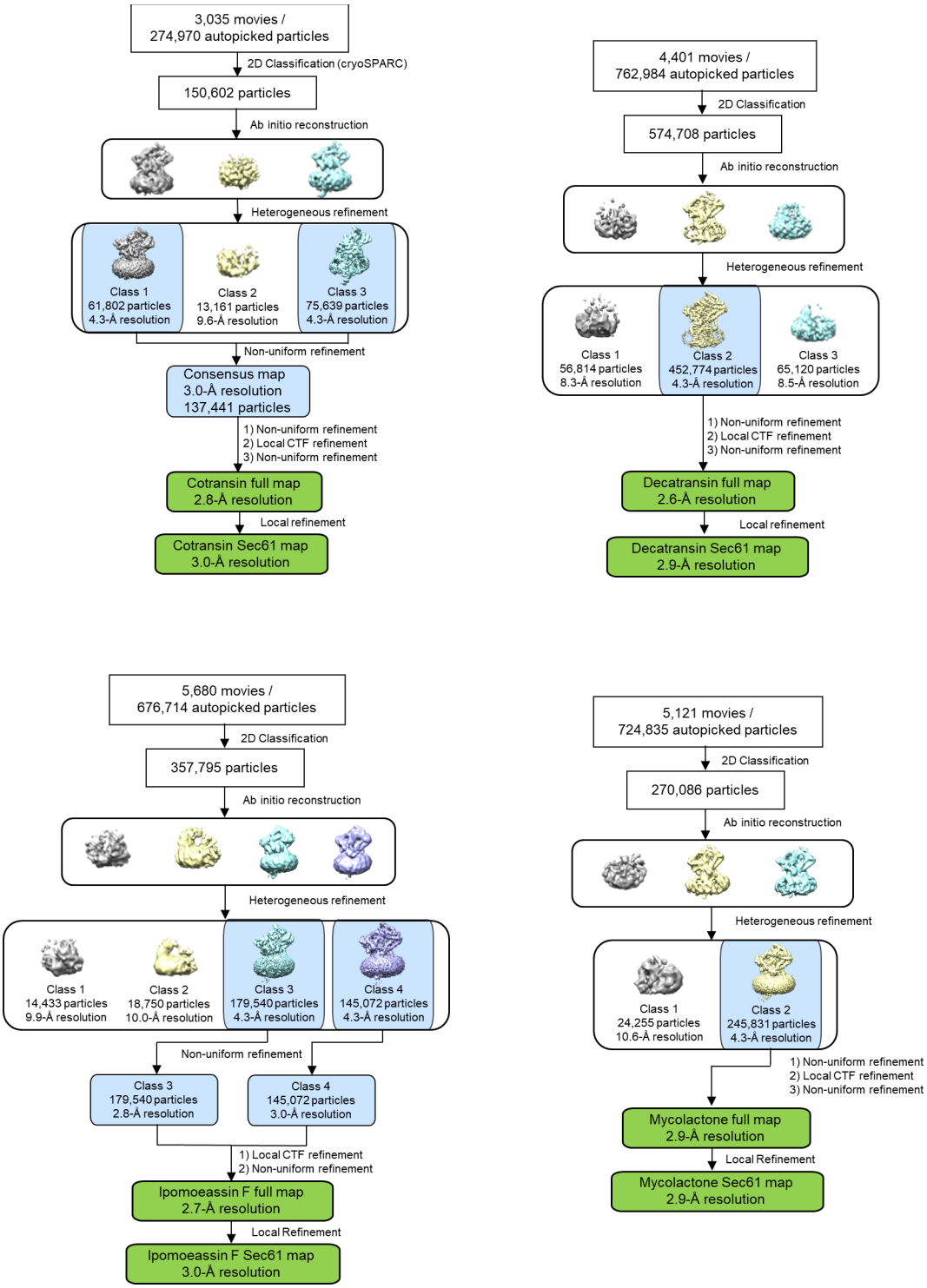

Supplementary Fig. S7. Additional schematics of single-particle cryo-EM image analysis workflow.
As in Supplementary Fig. S4b, but showing the datasets for the chimeric Sec complex in association with cotransin, decatransin, ipomoeassin F, or mycolactone.

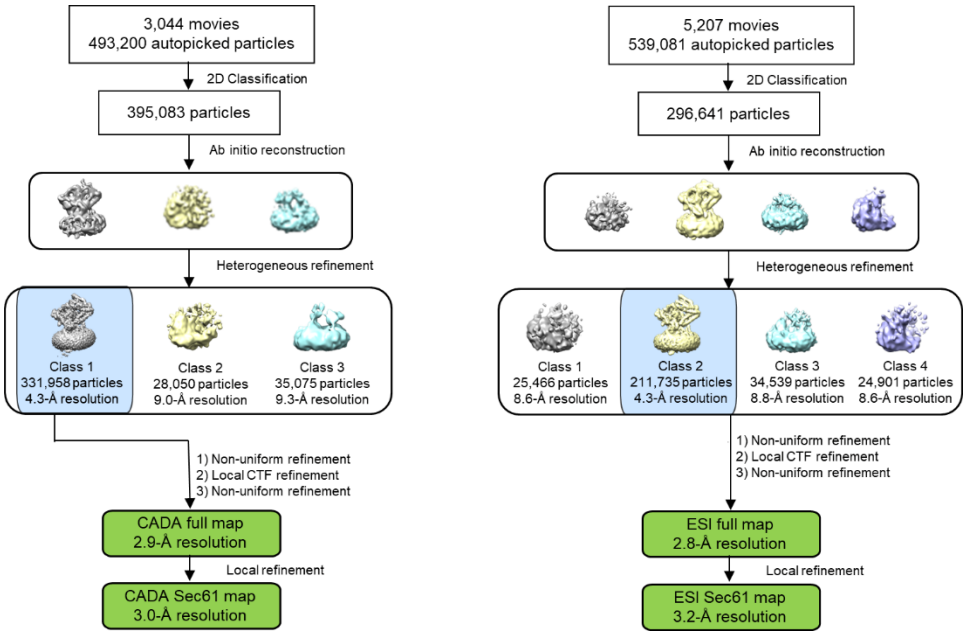

Supplementary Fig. S8. Additional schematics of single-particle cryo-EM image analysis workflow.
As in Supplementary Fig. S4b, but showing the datasets for the chimeric Sec complexes in association with CADA or ESI.

Supplementary Table S1. Cryo-EM data collection, refinement and validation statistics

	Sec61, Apo (class 1)	Sec61, Apo (class 2)	Sec61, Cotransin	Sec61, Decatransin	Sec61, Apratoxin F	Sec61, Mycolactone	Sec61, Ipomoeassin F	Sec61, CADA	Sec61, ESI
PDB accession ID	8DNV	8DNW	8DNX	8DNY	8DNZ	8DO0	8DO1	8DO2	8DO3
EMDB accession number	27581	27582	27583	27584	27585	27586	27587	27588	27589
Data collection and processing									
Magnification	81,000x	81,000x	81,000x	81,000x	81,000x	81,000x	81,000x	81,000x	81,000x
Voltage (kV)	300	300	300	300	300	300	300	300	300
Electron exposure (e^{-}/Å^2)	50	50	50	50	50	50	50	50	50
Defocus range (μm)	-0.8 to -1.6	-0.8 to -1.6	-0.8 to -1.6	-0.8 to -1.6	-0.8 to -1.6	-0.8 to -1.6	-0.8 to -1.6	-0.8 to -1.6	-0.8 to -1.6
Pixel size (Å)	1.05	1.05	1.05	1.05	1.05	1.05	1.05	1.05	1.05
Symmetry imposed	*C*1	*C*1	*C*1	*C*1	*C*1	*C*1	*C*1	*C*1	*C*1
Initial particle images (no.)	616,121	616,121	274,970	762,984	910,463	724,835	676,714	493,200	539,081
Final particle images (no.)	188,637	147,081	137,441	452,774	497,555	245,831	324,612	331,958	211,735
Map resolution (Å)	3.0	3.4	3.0	2.9	2.6	2.9	3.0	3.0	3.2
FSC threshold	0.143	0.143	0.143	0.143	0.143	0.143	0.143	0.143	0.143
Map resolution range (Å) (min. to 75 percentile)	2.6–7.4	2.9–7.5	2.6–7.6	2.4–6.4	2.3–6.4	2.6–7.5	2.6–7.6	2.3–7.2	2.7–6.9
Refinement									
Initial model used	PDB:8DNZ	PDB:8DNZ	PDB:7KAH	PDB:8DNZ	PDB:8DNX	PDB:8DNZ	PDB:8DNZ	PDB:8DNZ	PDB:8DNZ
Model resolution (Å)	3.2	3.5	3.1	3.0	2.7	3.1	3.2	3.1	3.4
FSC threshold	0.5	0.5	0.5	0.5	0.5	0.5	0.5	0.5	0.5
Map sharpening *B* factor (Å^2)	-91	-100	-78	-100	-77	-90	-99	-96	-104
Model composition									
Non-hydrogen atoms	4157	4060	4,271	4,331	4,337	4,247	4,339	4,226	4,185
Protein residues	535	528	543	549	551	542	551	541	534
Ligands	0	0	1	1	1	1	1	1	1
B factors (Å^2)									
Protein	76.57	49.58	71.46	41.25	63.60	52.92	65.58	49.43	61.03
Ligand	-	-	60.88	39.34	56.47	42.82	47.33	47.21	62.00
R.m.s. deviations									
Bond lengths (Å)	0.004	0.003	0.004	0.003	0.004	0.002	0.003	0.004	0.004
Bond angles (°)	0.593	0.515	0.579	0.597	0.513	0.489	0.560	0.650	0.582
Validation									
MolProbity score	1.51	1.30	1.47	1.47	1.32	1.40	1.67	1.38	1.43
Clashscore	7.53	5.57	6.35	7.65	5.90	7.31	10.10	6.98	6.70
Poor rotamers (%)	0	0	0	0	0	0.22	0.22	0.22	0
Ramachandran plot									
Favored (%)	0	0	0	0	0	0	0	0	0
Allowed (%)	2.48	1.36	2.63	2.22	1.29	1.69	2.76	1.69	2.30
Disallowed (%)	97.52	98.64	97.37	97.78	98.71	98.31	97.24	98.31	97.70

Supplementary Table S2. Effects of mutations in *Sc*Sec61 on yeast growth inhibition by cotransin, ipomoeassin F, and decatransin

			IC50 value (μM)		
ScSec61 aa position	Mutation	Position in HsSec61A1	Cotransin	Ipomoeassin F	Deca-transin*
	WT		0.87; 0.55[#]	0.06	3.1; 1.2*
47	G47D	C46	>200*		100*
63	L63D	F62	>200	0.40	
63	L63W	F62	0.43	0.25	
63	L63N	F62	>200	<0.06	2.9*
71	A71D	A70	1.4*		3*
72	S72F	S71	>200	0.17	>200*
79	E79K	E78	>200*		>200*
81	G81D	G80	>200*		3.6*
82	V82D	I81	>200	>100	
82	V82W	I81	>200		
84	P84L	P83	>200*		>200*
86	I86T	V85	0.54	<0.06	
86	I86D	V85	>200	<0.06	
86	I86W	V85	2.08		
87	T87I	T86	>200*		>200*
89	S89D	G88	1.10	<0.06	
89	S89W	G88	1.00	0.09	
90	M90D	L89	>200	>100	
90	M90W	L89	1.06	0.13	
93	Q93D	Q92	2.72	0.07	
93	Q93W	Q92	0.53	0.12	
96	Q96D	A95	0.77	<0.06	
96	Q96W	A95	1.10	0.07	
97	G97D	G96	0.62; 0.3*	1.48	>200*
97	G97W	G96	1.04	0.06	
111	R111D	R109	1.15	<0.06	
111	R111W	R109	0.87	<0.06	
115	Q115D	N113	1.84	<0.06	
115	Q115W	N113	1.05	<0.06	
129	Q129D	Q127	>200	0.28	
129	Q129W	Q127	>200	>100	
129	Q129L	Q127	0.58; 1.1[#]	18.3	>100
168	D168W	D166	0.22	<0.06	
172	S172D	Q170	1.09	<0.06	
172	S172W	Q170	0.88	0.07	
178	G178D	G176	1.18	<0.06	
178	G178W	G176	0.52	<0.06	
179	S179D	S177	1.03	<0.06	
179	S179W	S177	0.26	<0.06	
179	S179A	S177	0.82		
179	S179C	S177	0.68		
179	S179F	S177	0.56		
179	S179G	S177	0.80		
179	S179H	S177	1.00		
179	S179I	S177	0.53		
179	S179K	S177	0.57		
179	S179L	S177	1.03		
179	S179M	S177	1.01		
179	S179N	S177	1.04		
179	S179Q	S177	1.13		
179	S179R	S177	0.54		
179	S179S(=WT)	S177	0.91		
179	S179T	S177	0.98		
179	S179V	S177	0.80		
179	S179Y	S177	0.56		
181	I181D	I179	0.59	<0.06	
181	I181W	I179	<0.1		
182	S182D	S180	1.34	<0.06	
182	S182W	S180	>200	0.06	
185	T185D	I183	>200	>100	
185	T185W	I183	0.60		
186	A186T	A184	0.3*		2.4*
287	Y287D	Y285	>200		
287	Y287W	Y285	5.32		
291	T291W	I289	0.83	13.0	
291	T291D	I289	3.05	0.07	
294	M294D	I292	>200	>100	
294	M294W	I292	1.06		
296	Q296D	Q294	1.07	0.14	
296	Q296W	Q294	0.59	<0.06	
298	A298T	A296	>200*		>200*
302	N302L	N300	>200	>100	>100
302	N302D	N300	0.51	>100	
302	N302W	N300	>200	>100	
305	L305D	V303	>200	11.7	
305	L305W	V303	>200	<0.06	
307	S307D	S305	1.37	<0.06	
307	S307W	S305	>200	0.58	
307	S307F	S305	>200*		>200*
379	T379D	T378	1.07	0.09	
379	T379W	T378	0.59	<0.06	
380	W380D	W379	1.07	0.15	
382	E382D	E381	1.09	<0.06	
382	E382W	E381	1.70	<0.06	
384	S384D	S383	2.01	<0.06	
384	S384W	S383	0.60	0.19	
386	T386D	S385	1.44	<0.06	
386	T386W	S385	1.11	<0.06	
430	G430D	G429	0.5*		3.7*
446	A446T	T445	1.3*		2.7*
450	M450D	L449	4.04	0.87	
450	M450W	L449	2.15		
454	T454D	I453	0.46	<0.06	
454	T454W	I453	<0.1	<0.06	
461	A461D	I460	1.36		
461	A461W	I460	0.86		
480	M480D	L475	1.01		
480	M480W	L475	1.03		
multiple	ΔPlug (52-74→G)		>200	>100	
multiple	V82D/I86D/ M294K	I81/V85/ I292	>200		
multiple	V82D/I86D/ M450K	I81/V85/ L449	>200		
multiple	I181D/T185D /M450K	I179/I183/ L499	>200		
multiple	Q308/I323/ W326/L342A	Q306/L321/ W324/L341	>200		
multiple	I86T/Q308/ I323/W326/ L342A	V85/Q306/ L321/W324/ L341	>200		
multiple	Q96W/Q99H	A95/K98	0.89		

Gray highlight: IC50 larger than 5x but less than 100x of IC50 of WT.
Yellow highlight: IC50 larger than 100x of IC50 of WT.
Blank: not determined.
* Data from Junne et al., doi:10.1242/jcs.165746.
[#] Values measured with the strain BY4743Δ9aURA harboring pDQ1.